

# Comparative Study of the Synthesis of sub-10 nm Carbon-Supported Gold Nanoparticles and their Suitability for Methanol Electrooxidation in Alkaline Media

Emil Dieterich, Simon-Johannes Kinkelin, and Michael Bron<sup>\*[a]</sup>

**Abstract:** Gold nanoparticles were synthesized and supported on carbon, or directly synthesized on carbon according to five different methods reported in literature, aiming at particles < 10 nm. Characterization was done with transmission electron microscopy and thermogravimetric analysis. Although all syntheses yielded particles with an average diameter < 10 nm, the formation of few very large particles, where a relatively large amount of Au is buried, as well as loss during the supporting procedure led to the exclusion of

four of the five tested methods for further studies. The most promising AuNPs supported on carbon were tested for the methanol electrooxidation (MEO) in alkaline media. Four different Au-loadings were realized, and supporting led to moderate particle growth depending on the loading. To compare MEO activity of the samples with different Au-loadings a conversion factor was developed where the MEO activity can be compared in terms of NP size and Au-loading.

## Introduction

Gold nanoparticles (AuNPs) are of great interest for a broad variety of technologies, including catalysis, nano-electronics and biomedicine, because of their exceptional chemical stability, catalytic activity and unique size-dependent electronic and optical properties.<sup>[1,2]</sup> Among all sizes monodisperse sub 10 nm AuNPs are a very fascinating material. Their share of surface atoms is overtaking that of the bulk atoms, and as a consequence the atomic surface coordination decreases which leads to new catalytic properties, reactivity and stability.<sup>[3]</sup> For electrocatalytic applications, AuNPs are usually immobilized on a supporting material, for higher stability, practicality and synergetic catalytic effects of the support. Often used supporting materials are conductive carbons, including CNTs,<sup>[4]</sup> MWCNTs<sup>[4]</sup> and carbon blacks<sup>[5]</sup> as well as metal oxides like ZnO,<sup>[6]</sup> TiO<sub>2</sub><sup>[7]</sup> and SiO<sub>2</sub>.<sup>[6]</sup>

A large body of literature is available describing the synthesis of monodisperse AuNPs with particle diameters below 10 nm.<sup>[8–12]</sup> Supporting these previously synthesized gold nanoparticles is a non-trivial issue. To support AuNP on carbon, the particles usually are stirred with added carbon support followed by drying (50–120 °C, air or argon atmosphere). The dry product is usually treated, depending if/what sort of stabilizing agent is used in the synthesis.<sup>[12,13]</sup> These post-treatments are mainly


done for two reasons, first to increase the stability of the catalyst and second to remove surfactants (e.g. the stabilizer) and thus to liberate the gold surface, since any remaining surfactants could hinder surface reactions. Furthermore, some surfactants were shown to modify the selectivity of the catalyst.<sup>[13,14]</sup> However, depending on the treatment and supporting material, there is particle growth to be expected,<sup>[15]</sup> indicating that this treatment has to be done with great care.


In this study, we evaluate and compare various synthesis routes for sub 10 nm AuNP<sup>[4,8–11]</sup> towards applicability of the supported NP in electrocatalysis. A special focus is on the gold utilization during synthesis and supporting procedure and on the resulting electrocatalytic properties. Given the known issues of greenhouse gas emissions due to the burning of fossil fuels and the recent developments in the field of alkaline fuel cells (e.g., use of anion exchange membranes), there is re-growing interest in the electrochemical oxidation of small organic molecules, which may be used in direct alcohol fuel cell, for example.<sup>[16,17]</sup> Typical commercial catalysts for the direct alcohol fuel cell are PtNP based catalysts on carbon support, which are showing excellent activities for the MEO.<sup>[18]</sup> Because of the poisoning of Pt by CO (by-product of the alcohol oxidation) and also the high price of Pt and the comparably lower activity of Pt based catalysts in alkaline media there is an immense interest in Pt free catalysts.<sup>[18,19]</sup> Due to this, the electrocatalytic oxidation of methanol (MEO)<sup>[20]</sup> has been chosen as a test reaction in this study.

## Results and Discussion

Five different methods reported in literature were used for AuNP synthesis. In methods 1–3, AuNP were preformed using reducing agents and stabilizer, and the preformed AuNP were then transferred onto a carbon support. In methods 4 and 5, the AuNP were directly synthesized on carbon support. All

[a] E. Dieterich, S.-J. Kinkelin, Prof. Dr. M. Bron  
Institut für Chemie, Technische Chemie I  
Martin-Luther-Universität Halle-Wittenberg  
Von-Danckelmann-Platz 4, 06120 Halle (Germany)  
E-mail: michael.bron@chemie.uni-halle.de

 Supporting information for this article is available on the WWW under <https://doi.org/10.1002/cnma.202200098>

 © 2022 The Authors. ChemNanoMat published by Wiley-VCH GmbH. This is an open access article under the terms of the Creative Commons Attribution Non-Commercial NoDerivs License, which permits use and distribution in any medium, provided the original work is properly cited, the use is non-commercial and no modifications or adaptations are made.

syntheses were aiming at Au particle sizes < 10 nm. As reducing agents NaBH<sub>4</sub> or KBH<sub>4</sub> were used, while 1-dodecanethiol (1-DDT), polyvinylpyrrolidone or no capping agent was applied to control particle growth, depending on the method. Details on the synthesis methods can be found in the experimental part.

STEM and TEM images were recorded to evaluate the size and size distribution of AuNPs after synthesis as well as supported on carbon material. Figure 1 shows TEM images of the synthesized AuNP, while Table 1 presents the statistical evaluation of these images. The TEM images show a distribution of gold particle sizes from 1.1 to 182 nm (Supporting Information (SI) Figure 1f) for method 1 (synthesis according to Jana et al.<sup>[9]</sup>). While most Au particles are in the targeted size range of < 10 nm (SI Figure 2a)), still a major loss of gold occurs to particles which are not in the targeted size range (if 1 out of 600 AuNPs is in the range of ~182 nm, the loss is around ~96%<sub>Au</sub>). While the average particle size agrees with the literature, the standard deviation differs from the reported values. For the synthesized AuNP according to method 1 a color change from light- to dark-red was observed over the next few hours, which indicates a particle growth.<sup>[21]</sup> The AuNPs synthesized according to method 2 – Martin et al.<sup>[8]</sup> and method 3 – Brust et al.<sup>[10]</sup> are well within the targeted size range (1.1–10.9 nm and 0.6–7.5 nm) with an average size and a small standard deviation of 3.8 nm (± 1.0 nm) or 2.3 nm (± 0.6 nm) (SI Figure 2a)). Both results are in close agreement to the literature, and no changes in color were observed afterwards. The AuNPs synthesized according to method 3 are stable for at least eight months (SI Figure 3, 4 and SI Table 2). Their size can be changed by varying the length of the carbon-chain of the stabilizer used during synthesis (SI Figure 5 and SI Table 3). Due to the formation of large Au particles, method 1 was not further considered for Au/C catalyst preparation.

TEM images of Au/C are shown in Figure 2 while Table 2 shows the evaluation of the TEM images and the TG measurements. Au/C synthesized according to method 4 – Marshall et al.<sup>[11]</sup> (Figure 2c) and g)) and method 5 – Zhang et al.<sup>[22]</sup> (Figure 2d) and h)) shows a broader size range and AuNPs >

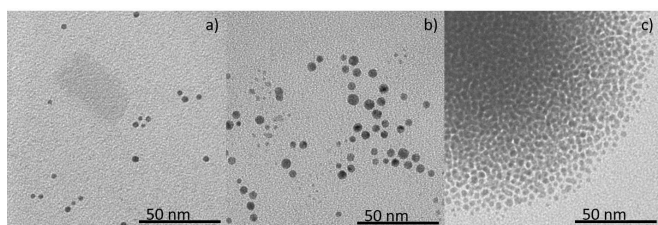


Figure 1. Representative TEM images of AuNPs synthesized according to a) method 1; b) method 2 and c) method 3.

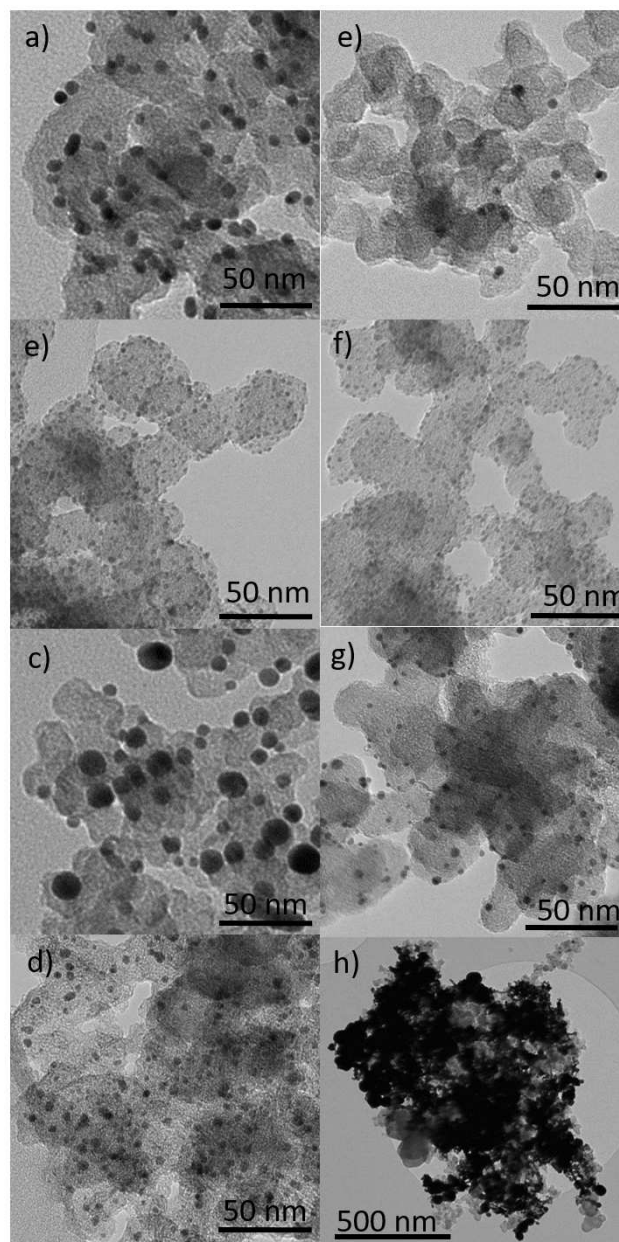


Figure 2. TEM images of the treated Au/C samples synthesized according to a), e) method 2; b), f) method 3; c), g) method 4 and d), h) method 5.

10 nm. Method 5 shows agglomerations of gold up to a few micrometers (Figure 2h)). More than 95% of the particles are in the targeted size range (size distribution for particles < 10 nm SI Figure 2b)), still the particles > 10 nm imply a big loss of gold in particles much larger than the targeted size range.

Table 1. Sizes and size ranges of freshly synthesized gold particles.

method	Average size (stdv.) in nm	Size range in nm	Particles measured	Reported size in nm
1	3.4 (± 5.8)	1.1–182	1006	3.5 (± 0.7) <sup>[9]</sup>
2	3.8 (± 1.0)	1.1–10.9	3747	4.8 <sup>[8]</sup>
3	2.3 (± 0.6)	0.6–7.5	1800	2.0–2.5 <sup>[10]</sup>

**Table 2.** Size, size range and transfer rate of the amount of gold used in the syntheses related to the amount of Au on the supporting material after Au/C sample treatment. Reported sizes in nm for method 4–4.7 nm<sup>[11]</sup> and method 5–6.7 nm (size range 2–16 nm)<sup>[22]</sup>.

Method	Average size (stdv.) in nm	Size range in nm	Particles measured	Transfer rate in % (stdv.)
2	4.3 (± 1.0)	1.1–11.2	761	26 (± 23)
3	3.9 (± 1.3)	0.8–9.2	7053	76 (± 6)
4	4.1 (± 1.6)	0.8–18.1	662	169 (± 79)
5	6.3 (± 21)	1.3–449	646	102

During the supporting process, the mean particle sizes of the AuNPs synthesized according to method 2 and method 3 grew from 3.8 to 4.3 nm respectively 2.3 to 3.9 nm (see Figure 2a), e), b) and f)). Another important aspect is the amount of transferred gold during the synthesis and supporting process, which is determined from the Au-loading on Vulcan XC72 as examined by TG measurement (SI Figure 6 and SI Table 1). In Table 2 the fractions of transferred gold are shown. Transfer rates above 100% for the products according to method 4 and 5 are presumably the result of loss of carbon material during the synthesis. The carbon supported AuNPs show transfer rates between 26 and 76% (method 2 and 3, respectively). None of the synthesized Au/C products show a fully homogenous distribution of the AuNP on the supporting material (Figure 2). Some of the TEM images may suggest a homogenous particle distribution on the supporting material but there are areas on the supporting material without AuNPs, also in TEM images not shown. This is presumably related to inhomogeneous surface properties of the supporting material. To conclude, Au/C synthesized according to method 3 and then supported on Vulcan XC72 and treated as described shows only AuNPs in the targeted size range (i.e., no loss of material buried in large AuNPs) and an average loss of only ~24% during the synthesis and supporting procedure. Therefore, this catalyst was used for all further syntheses and investigations.

After establishing the most suitable preparation procedure for well-defined Au/C electrocatalysts with Au particle size < 10 nm, the Au-loading on Vulcan XC72 has been varied in order to evaluate its influence on the properties of Au/C in the MEO in alkaline electrolyte. Catalysts with four different Au-loadings were prepared. Table 3 shows the particle sizes, standard deviations, size ranges (from TEM, SI Figures 1 and 7), Au-loadings (from TG measurements) and the electrochemical surface area (ECSA) normalized by the total catalyst weight, as detailed in the SI. Around 97% of the AuNPs are < 10 nm and none are > 13 nm (SI Figure 7). As mentioned above, generally the AuNPs don't show a homogenous distribution on the supporting material (compare SI Figure 1c)).

As mentioned above, the interest in the electrooxidation of small organic molecules is ongoing given the possibility of establishing CO<sub>2</sub>-neutral energy conversion cycles, in case the organic molecules are prepared from renewable resources and converted in e.g. fuel cells. Recent progress in the field of alkaline fuel cells (in particular, progress in alkaline exchange membranes) together with the known electrocatalytic activity of gold in alkaline solution (in comparison to acids, where it is rather inactive) motivated us to investigate the properties of Au/C prepared as mentioned above towards the MEO. The four catalysts prepared with different Au-loadings were investigated towards the MEO using cyclic voltammetry in different electrolyte solutions (0.1 M KOH as base electrolyte, and with addition of 0.5 M, 2 M or 5 M MeOH). Figure 3 shows cyclic voltammograms (CVs) of one of the catalysts in the electrolyte solutions with different MeOH concentrations (Figure 3b)) and all four catalysts in the same solution (5 M MeOH, Figure 3a)). In 0.1 M KOH four potential regions with different contributions of Faradaic currents may be distinguished (SI Figure 8), namely the gold oxidation (Au-ox.) and the carbon corrosion (both in the forward scan, i.e. scan to more positive potentials), the gold reduction (Au-red.) in the backward scan and the OH<sup>-</sup> desorption. Obviously, the Au-ox. and carbon corrosion are overlapping. In MeOH-containing KOH electrolyte, as expected a different behavior is observed. In the forward scan the MEO is overlapping with the Au-ox., and in the backward scan the Au-red. is overlapping with the MeOH-ox. and probably the oxidation of reaction intermediates.<sup>[12,23–25]</sup> The CVs show an increase of the MeOH- and Au-ox. peak current with higher Au-loading and a higher MEO peak current with increasing MeOH concentration in the electrolyte. Also the oxidation peaks in the backward scan are increasing with both, higher Au-loading and higher MeOH concentration in the electrolyte. Interestingly, in the electrolyte solutions with higher MeOH concentration the MEO starts already at potentials below 0 V, i.e. below the potential where Au is oxidized. We assume that OH<sup>-</sup> adsorption might aid in the MeOH oxidation at less positive potentials. Furthermore, from the CVs it seems that progressing Au-ox.

**Table 3.** Particle sizes, size ranges and metal amount of Au/C together with the intended Au-loading as well as the electrochemical surface area (ECSA) calculated from the Au reduction peak of the catalysts used in electrocatalytic experiments.

catalyst	Average size (stdv.) in nm	Size range in nm	Amount of Au in wt.% (theoretical wt.%)	ECSA in m <sup>2</sup> /g <sub>cat.</sub>
Au/C-1.7	2.9 (± 1.3)	0.8–9.2	1.7 (2.5)	0.12
Au/C-3.6	3.1 (± 1.0)	1.2–9.0	3.6 (5.0)	0.21
Au/C-8.3	4.4 (± 1.4)	1.1–12.2	8.3 (10.0)	0.64
Au/C-25	5.1 (± 1.7)	1.5–12.3	25.0 (24.0)	2.35

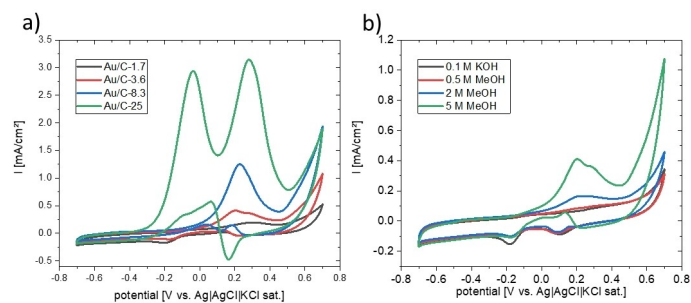


**Figure 3.** 25<sup>th</sup> cycle from CVs, a) Au/C catalysts in 5 M MeOH and 0.1 M KOH electrolyte; b) Au/C-3.6 in the four different used electrolyte solutions (0.1 M KOH as well as 0.5 M, 2 M and 5 M MeOH in 0.1 M KOH).

inhibits MeOH-ox., as seen by the decrease in oxidation current above ~0.5 V, and only at very positive potentials the current rises again, which might be an overlap between MeOH-ox. on oxidized Au at high overpotentials and carbon corrosion.

Notably, during the CV measurement of Au/C-25 there is a fifth Faradaic peak building up and reaching a stable level after 15 cycles with a maximum at around -0.05 V (Figure 3a) and SI Figure 9 and 10). In literature, intermediates/products of the MEO reaction which could be oxidized further are formaldehyde, formate and CO.<sup>[26]</sup> CV measurements of solutions containing these intermediates did not show peaks at the observed potential for Au/C-25, thus we suspect that accumulation of these intermediates are not responsible for the slow generation of this new oxidation peaks (SI Figure 11). In detail, formate is oxidized around 0.3 V. For the measurement of formaldehyde in the electrolyte there is an oxidation current observed starting very early at -0.47 V and, as literature predicts, a formate peak is observed also, as formate is a known oxidation product of formaldehyde.<sup>[26,27]</sup> CVs of CO saturated electrolyte do not show significant additional peaks, as literature suggests.<sup>[28,29]</sup> A local pH change was also considered, but considered unlikely since the pH-dependent carbon corrosion at higher potentials seems to be unchanged. CVs under rotation of the electrode however seem to indicate that forced convection leads to a depletion of the responsible species in the vicinity of the surface, as seen by a decrease of the peak with increasing rotation rate at the Au/C-25 catalysts (SI Figure 9b)). Considering possible reaction pathways and intermediates for the MEO<sup>[12,23,30-32]</sup> we suggest a change of selectivity with a higher Au-loading, which we assume to result from the smaller particle distances. We can only speculate that a high concentration of intermediates (e.g. formaldehyde),

which is build up locally, leads to solution chemistry and formation of intermediates, which then yield the unexpected CV peak.

It is not an unexpected result that the catalysts with higher Au-loading show higher MEO currents and ECSA. However, to quantitatively compare the different catalysts, we defined a conversion factor (cf) (SI section 1.2). This factor displays the capability to oxidize MeOH (both forward and backward scan) as normalized by the Au-red. electrical charge, which lets us compare the MeOH-ox. activity with regard to particle size and Au-loading. This comparison is valid as long as the MEO mechanism of the different catalysts are similar. Thus, the data for Au/C-25 has to be considered with caution, since the developing peak likely does not stem from initial MeOH-ox. To estimate the activity for MeOH-ox. thus, only the charges from the peak at approx. 0.2–0.3 V were used to calculate the cf of Au/C-25. Figure 4 shows the cf and the particle size in dependence of the Au-loading. For Au/C-1.7, -3.6 and -8.3 it is reasonable to assume the same MEO mechanism from the very same CV behavior. For these catalysts clearly the cf is changing with the Au-loading and is having a maximum for Au/C-3.6, and this behavior is valid for all three different MeOH concentrations used in this study. The electrochemical surface<sub>ECSA</sub> specific current density shows the same behavior, i.e. is highest for Au/C-3.6, as displayed in Table 4, 5<sup>th</sup> column. On the other hand, the mass and the surface<sub>GCE</sub> specific current densities (i.e., related to geometrical surface area) are showing a different

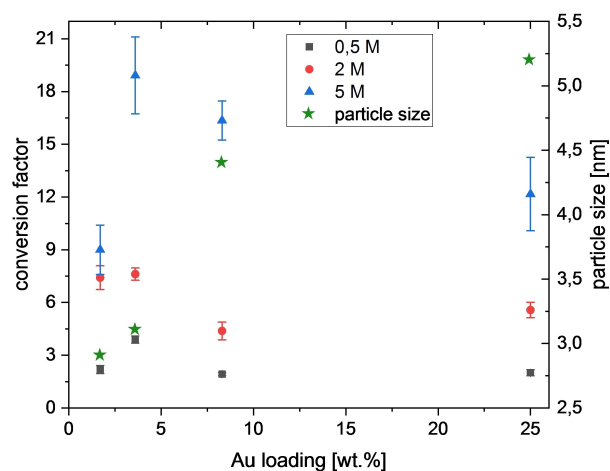


**Figure 4.** Conversion factor (cf) extracted from CV and particles size vs. the Au-loading for MEO over Au/C catalysts for all three MeOH concentrations used.

**Table 4.** MEO maximum current (5 M MeOH electrolyte corrected by the corresponding measurement in 0.1 M KOH) normalized by the geometric electrode area (0.1256 cm<sup>2</sup>), normalized by the amount of gold and by the calculated ECSA, as well as oxidation charge related to amount of gold.

catalyst	surface <sub>GCE</sub> specific current density in mA/cm <sup>2</sup>	mass specific oxidation charge density in mC/mg <sub>Au</sub>	mass specific current density in mA/mg <sub>Au</sub>	surface <sub>ECSA</sub> specific current density in mA/cm <sup>2</sup>
Au/C-1.7	0.14	263.42	55.59	0.76
Au/C-3.6	0.50	443.10	92.97	1.59
Au/C-8.3	1.39	439.75	111.27	1.44
Au/C-25	3.83	410.20	102.10	1.09

behavior, which can be explained by the fact, that only the peak currents of the CVs are taken into account, and not the whole oxidation charge. If the oxidation charge is considered (Table 4, 3<sup>rd</sup> column), again the Au/C-3.6 catalyst shows the best performance. These considerations also emphasize the advantage of the cf, which uses all oxidation charge (forward and backward scan) compared to the consideration of only the mass or surface<sub>GCE</sub> specific peak current densities to compare the catalysts.

Keeping in mind the different particle sizes of these catalysts, this observation might point to a particle size effect in MEO on gold. On the other hand, the differences in average particle sizes between Au/C-1.7 and Au/C-3.6 are small. In literature MEO mass specific oxidation currents have been reported to increase with the Au-loading,<sup>[33]</sup> which is in contrast to our results.

We would like to emphasize again that we have carefully chosen a catalyst preparation procedure leading to high Au utilization and low Au losses, which might explain the higher values compared to literature. While the mass specific and the surface<sub>GCE</sub> specific current densities show different behaviors, the cf values indicate a non-monotonous effect of the Au-loading which is supported by the behavior of the surface<sub>ECSA</sub> specific current and emphasizes the advantage of using the charge instead of the maximum current for catalyst comparison. Furthermore, also with increasing average particle size the cf is decreasing. Thus we conclude that for optimum MEO on supported gold nanoparticles, both particle size and loading on the carbon have to be adjusted.

## Conclusion

In this study, different synthesis methods reported in literature for the preparation of AuNP and Au/C catalysts are investigated. All synthesis routes yield AuNPs in the average sizes reported in the respective literature. However, for method 1, 4 and 5 a high loss of gold to particles > 10 nm and for method 2 a high loss of gold during the supporting process are observed, rendering these methods inappropriate for fundamental studies in electrocatalysis. The most suitable approach was method 3 (a synthesis procedure according to Brust et al.), with a relatively small Au loss during synthesis and very moderate increase in size during the supporting process (average particle size 2.3 nm, supported 3.9 nm; size range 0.8–12.3 nm). Also the particles show only minor size changes during storage and their size can be manipulated by changing the stabilizing agent, which makes them even more interesting for a wide range of applications.

The mentioned nanoparticles were employed to prepare four Au/C catalysts with different Au-loadings, which led to a moderate, but loading-dependent growth of the nanoparticle sizes. To compare the catalysts towards MEO, a conversion factor (cf) was defined, which takes into account the different exposed surface areas of the catalysts. The cf for the catalyst with an Au-loading of 3.6 wt. %<sub>Au</sub> is the highest and suggests that the activity for the MEO from a combination of this Au-loading and particle size is optimal. All four catalysts show

higher current per cm<sup>2</sup> and current per mg<sub>Au</sub> peak values for the MeOH-ox. than comparable Au/C catalysts in literature.<sup>[33]</sup> Compared to commercial Pt/C catalysts (170 mA/mg<sub>Pt</sub>, 20 wt.%<sub>Pt</sub>, ECSA 28 m<sup>2</sup>/g<sub>cat.</sub>) the mass specific current of the Pt/C catalysts is higher what could be explained by their much larger ECSA.<sup>[34]</sup> Therefore, further studies should investigate how to increase the ECSA of Au/C and take into account possibly present surfactants e.g. stabilizer which could decrease the ECSA.<sup>[35]</sup> An unexpected peak was observed for the catalysts with an Au-loading of 25 wt.%<sub>Au</sub>. Investigations of typical intermediates of the MEO could not clarify the origin of this peak and it probably results from locally high intermediate concentration and small particle distances on the support.

## Experimental Section

### Chemicals

The following chemicals and materials were used as received: HCl (37%, ROTH), HNO<sub>3</sub> (65%, ROTH), ethanol (abs. HPLC, Th Geyer), DI H<sub>2</sub>O (SG water Ultra Clear UV ultrapure water, 0.055 μS\*cm<sup>-1</sup>), HAuCl<sub>4</sub>·3 H<sub>2</sub>O (ACS 99.99% metal basis, Au 49.0% min, Alfa Aesar), NaBH<sub>4</sub> (99%, Acros Organics), 1-dodocanethiol (> 98%, Sigma Aldrich), potassium iodide (≥ 9.5% ROTH), toluene (> 99.5% for synthesis, ROTH), NaOH (> 99%, ROTH), acetone (99.5% for synthesis, ROTH), n-hexane (> 99% p.a. ACS, ROTH), tetra-n-octylammonium bromide (98+ %, Alfa Aesar), Vulcan XC72 (carbon black, Cabot), polyvinylpyrrolidone K-30 (Sigma Aldrich), NH<sub>4</sub>OH (Rotipura, ROTH), KBH<sub>4</sub> (99.98%, ROTIMETIC), methanol (99.98%, ROTH), Nafion 117 (sol. 5%, Sigma Aldrich), potassium formate (≥ 9%, Sigma Aldrich), formaldehyde (37%, ROTH), CO (10.21% in He, Air Liquide).

### Instruments and measurements

Instruments used during the synthesis of nanoparticles include a rotary evaporator (Heidolph G3) and a centrifuge (Eppendorf 5804). Transmission electron microscopy (TEM) was performed on a Zeiss, Leo 912 Omega (120 keV, specific point-resolution 0.37 nm) and scanning transmission electron microscopy on a Zeiss GeminiSEM 500 with EDX (Oxford Ultim Max & Oxford Extreme and EBSD, Oxford C-Nano), resolution: 0.5 nm at 15 kV; 0.9 nm at 1 kV, 1.0 nm at 500 V, accelerating voltage: 0.02–30.0 kV, magnification: 50 times to 2,000,000 times, high efficiency InLens secondary detector for ultra-high resolution surface information). For the measurements the sample was suspended in ethanol and drop-casted onto carbon-coated copper grids, followed by drying at room temperature.

Thermogravimetric measurements were done to evaluate Au-loading in the supported catalysts and were performed with a Netzsch STA 449 F1 thermobalance. ~10 mg of sample were placed in a crucible (Al<sub>2</sub>O<sub>3</sub>) followed by heating (10 K/min) in 20% O<sub>2</sub>/Ar up to 1000 °C.

Cyclic voltammetry was carried out using a Metrohm Autolab PGSTAT 128 N. For the measurement a four-neck one-compartment glass cell with three electrodes immersed into 0.1 M KOH electrolyte with/without 0.5 M, 2 M or 5 M MeOH, flushed with N<sub>2</sub> for 20 min, was used. An Ag|AgCl|KCl<sub>sat.</sub> electrode (Meinsberger) was used as reference electrode, a Pt-net or Au-net as counter electrode and a freshly polished (1 μm, 0.3 μm Al<sub>2</sub>O<sub>3</sub> powder and DI H<sub>2</sub>O on fleece) catalyst coated glassy carbon electrode (GCE, A = 0.126 cm<sup>2</sup>)

as working electrode. The working electrode was prepared by dispersing the sample with a loading of 2.7 mg/ml (ratio 977/23 EtOH/Nafion 117) under sonication (Bandelin Sonocool, 75% intensity) for 15 min. Then 3.5  $\mu\text{l}$  were drop casted onto the GCE twice and dried at RT (resulting loading 150  $\mu\text{g cm}^{-2}$ ). Cyclic voltammetry was performed between  $-0.7$  and  $0.7$  V vs. Ag|AgCl|KCl<sub>sat</sub>. (all potentials are given relative to Ag|AgCl|KCl<sub>sat</sub>). The following procedure was applied: three CV cycles with a scan rate of 20 mVs<sup>-1</sup> were followed by 20 cycles with 500 mVs<sup>-1</sup>. After repeating this, another three cycles with 20 mVs<sup>-1</sup> were recorded. The rotating disc electrode (Radiometer, motor BM-ED1101) measurements were carried out as follows, 15 cycles with 20 mVs<sup>-1</sup>, followed by 2 cycles at each rpm (rpm in the order 400, 900, 1600, 900 and 400).

## Synthesis

Numerous syntheses for sub 10 nm AuNPs are reported in the literature, which provide a large variety of AuNPs with different or no surfactants. A selection of these (Martin et al.,<sup>[8]</sup> Jana et al.,<sup>[9]</sup> Brust et al.,<sup>[10]</sup> Marshall et al.,<sup>[11]</sup> and Zhang et al.<sup>[12]</sup>) was used for this study and the resulting AuNP were supported on Vulcan XC72 carbon black. All glassware was pre-cleaned in aqua regia under stirring for 12 h followed by heating up to 50 °C with reflux cooling. Afterwards all glassware was flushed with DI water and boiled in DI water for at least 1 h. All solutions were prepared with DI water or abs. EtOH. All syntheses were performed at least three times, except the synthesis according to Zhang et al.<sup>[12]</sup>

The first synthesis, referred to as method 1, was a modified procedure of Jana et al.<sup>[9]</sup> for 3.5 nm thiol-capped AuNPs. Briefly 20 ml of 0.25 mmol/l HAuCl<sub>4</sub>·3 H<sub>2</sub>O were stirred in a 100 ml one-neck flask. 0.6 ml of 0.1 M NaBH<sub>4</sub>, freshly prepared, was added dropwise and stirred for 15 min. 20.6  $\mu\text{l}$  of 1-DDT were added and stirred for 1 h. 40 mg potassium iodide and 2 ml toluene were added, followed by 3 min of vigorous shaking. The toluene phase was collected and stored at 4 °C.

The second synthesis – method 2 – was performed according to Martin et al.<sup>[8]</sup> Two stock solutions, 50 mmol/l HAuCl<sub>4</sub>·3 H<sub>2</sub>O with the same molar ratio of HCl and 50 mmol/l NaBH<sub>4</sub> with the same molar ratio of NaOH where prepared. 9.5 ml DI water were stirred (350 rpm) in a 50 ml beaker. 100  $\mu\text{l}$  of HAuCl<sub>4</sub> stock solution where added, followed by addition of 425  $\mu\text{l}$  of NaBH<sub>4</sub> stock solution. The dispersion was boiled for 3 min and cooled down to RT in a water bath before it was transferred to a 100 ml one-neck flask. 6.33 ml acetone were added followed by 7.58 ml n-hexane; in between and after the single additions the dispersion was mixed vigorously. The organic phase was collected and stored at 4 °C.

The third synthesis, referred to as method 3, was modified after Brust et al.<sup>[10]</sup> A solution of 184.5 mg tetraoctylammoniumbromide in 6.75 ml toluene was stirred at 350 rpm. 3.75 ml freshly prepared 0.03 M HAuCl<sub>4</sub>·3 H<sub>2</sub>O were added dropwise and stirred for 10 min, followed by the addition of 81  $\mu\text{l}$  1-DDT and then the addition of 3125  $\mu\text{l}$  freshly prepared 0.4 M NaBH<sub>4</sub> within 2 s and then 2 h of stirring to complete the reaction. After decanting the organic phase, the volume was reduced to one tenth by a rotary evaporator (55 °C, ~120 mbar), followed by adding 40 ml of EtOH and storing at 4 °C for 16 h. The precipitate was separated by centrifugation (5000 rpm, 30 min) and washed with EtOH twice. The product was dispersed in 3 ml toluene, 7 ml of EtOH were added, and the dispersion was stored at 4 °C.

The fourth method is according to Marshall et al.<sup>[11]</sup> where the AuNPs are directly transferred onto the carbon support. The required amount of Vulcan XC72 (114.2 mg), depending on the loading (here 20 wt. %<sub>Au</sub>), was suspended in DI water (10 ml H<sub>2</sub>O

per 100 mg supporting material) for 5 h in an ultrasonic bath (100 ml one-neck flask). Two stock solutions of 50 mmol/l HAuCl<sub>4</sub>·3 H<sub>2</sub>O with the same molar ratio of HCl and 50 mmol/l NaBH<sub>4</sub> with the same molar ratio of NaOH were prepared. 28 ml of DI water were mixed with 0.61 ml of the HAuCl<sub>4</sub>-stock solution in a 100 ml one-neck flask. 0.83 ml of the freshly prepared NaBH<sub>4</sub>-stock solution were added. This particle dispersion was added to the carbon dispersion and stirred for 20 h. The product was filtrated and washed with 100 ml DI water and dried at 60 °C overnight.

Method 5 is a modified synthesis according to Zhang et al.<sup>[12]</sup> where the AuNPs are synthesized directly on the carbon support. 160.7 mg Vulcan XC72 was filled into a 1 l one-neck flask while 56.7 mg HAuCl<sub>4</sub>·3 H<sub>2</sub>O where added to a second 1 l one-neck flask. To the latter flask, 300 ml DI water and 1.598 g PVP K-30 followed by another 180 ml DI water were added. The mixture was stirred until the PVP K-30 dissolved well. This Au-solution was added to the carbon support, stirred for 10 min and then suspended in an ultrasonic bath for 1 h. The pH of the dispersion was 3.2. 1 M NH<sub>4</sub>OH was added until the pH value reaches 9.3, followed by addition of 25 ml freshly prepared 0.6 M KBH<sub>4</sub> solution. The dispersion was stirred for 24 h, centrifuged (5000 rpm, 90 min) and washed with 80 ml DI water. The washing was repeated three times. After the washing, the product was dried at 60 °C for 15 h.

## Supporting of AuNP on Vulcan XC72

To support the prepared particles on Vulcan XC72 a method modified after<sup>[36]</sup> was used. The required amount of carbon black was dispersed by sonication in n-hexane (20 ml/100 mg n-hexane/carbon black) for 6 h. The respective AuNP suspension was dispersed by sonication for 30 min. Then it was added to the carbon black dispersion, sonicated again for 30 min and stirred overnight. The dispersion was separated by centrifugation (5000 rpm, 30 min) and washed with ethanol, followed by drying at 60 °C and ~500 mbar overnight. The product was a black powder, labelled Au/C. All supporting processes were done at least three times for the different AuNP syntheses. The theoretical Au-loading was, if not mentioned otherwise, 20 wt. %<sub>Au</sub>.

## Catalyst treatment

The literature reports different treatment methods for Au/C which aim to increase the stability and remove surfactants from the gold surface.<sup>[6,36–38]</sup> In this work, the Au/C catalysts were treated at 300 °C with 20% O<sub>2</sub>/Ar for 1 h followed by 2 h at 400 °C under 15% H<sub>2</sub>/Ar atmosphere in a tube-furnace. The total gas flow was 6 l/h with a heating ramp of 10 K/min. Before the heating ramp was started, the quartz glass tube with the quartz glass vessel, in which the sample was placed, was flushed with Argon (6 l/h) for 30 min.

## Acknowledgements

We thank Annett Quetschke (Institut für Chemie, Technische Chemie I, Martin-Luther-Universität Halle Wittenberg) for performing TEM and TG measurements and Frank Syrowatka (Interdisziplinäres Zentrum für Materialwissenschaften, Martin-Luther-Universität Halle-Wittenberg) for the STEM measurements. Dr. Matthias Steimecke (Institut für Chemie, Technische Chemie I, Martin-Luther-Universität Halle Wittenberg) is acknowledged for in-depth scientific discussions. Open Access funding enabled and organized by Projekt DEAL.

## Conflict of Interest

The authors declare no conflict of interest.

## Data Availability Statement

The data that support the findings of this study are available from the corresponding author upon reasonable request.

**Keywords:** electrochemistry · gold nanoparticles · methanol electrooxidation · supported catalysts · synthesis design

- [1] M.-C. Daniel, D. Astruc, *Chem. Rev.* **2004**, *104*, 293–346.
- [2] W. Kurashige, Y. Niihori, S. Sharma, Y. Negishi, *Coord. Chem. Rev.* **2016**, *320–321*, 238–250.
- [3] J. Piella, N. G. Bastús, V. Puentes, *Chem. Mater.* **2016**, *28*, 1066–1075.
- [4] R. Zhang, M. Hummelgård, H. Olin, *Mater. Sci. Eng.* **2009**, *158*, 48–52.
- [5] J. Luo, M. M. Maye, N. N. Kariuki, L. Wang, P. Njoki, Y. Lin, M. Schadt, H. R. Naslund, C.-J. Zhong, *Catal. Today* **2005**, *99*, 291–297.
- [6] G. Li, D.-E. Jiang, C. Liu, C. Yu, R. Jin, *J. Catal.* **2013**, *306*, 177–183.
- [7] A. Primo, A. Corma, H. García, *Phys. Chem. Chem. Phys.* **2011**, *13*, 886–910.
- [8] M. N. Martin, J. I. Basham, P. Chando, S.-K. Eah, *Langmuir* **2010**, *26*, 7410–7417.
- [9] N. R. Jana, L. Gearheart, C. J. Murphy, *Langmuir* **2001**, *17*, 6782–6786.
- [10] M. Brust, M. Walker, D. Bethell, D. J. Schiffrin, R. Whyman, *J. Chem. Soc. Chem. Commun.* **1994**, *0*, 801–802.
- [11] A. T. Marshall, V. Golovko, D. Padayachee, *Electrochim. Acta* **2015**, *153*, 370–378.
- [12] S. Yan, S. Zhang, Y. Lin, G. Liu, *J. Phys. Chem. C* **2011**, *115*, 6986–6993.
- [13] B. Donoeva, P. E. de Jongh, *ChemCatChem* **2018**, *10*, 989–997.
- [14] Z. Niu, Y. Li, *Chem. Mater.* **2014**, *26*, 72–83.
- [15] L. Prati, A. Villa, *Acc. Chem. Res.* **2014**, *47*, 855–863.
- [16] A. S. Aricò, P. Bruce, B. Scrosati, J.-M. Tarascon, W. van Schalkwijk, *Nat. Mater.* **2005**, *4*, 366–377.
- [17] J. Hou, Y. Shao, M. W. Ellis, R. B. Moore, B. Yi, *Phys. Chem. Chem. Phys.* **2011**, *13*, 15384–15402.
- [18] S. S. Siwal, S. Thakur, Q. B. Zhang, V. K. Thakur, *Mater. Today Chem.* **2019**, *14*, 100182.
- [19] Z. Yin, H. Zheng, D. Ma, X. Bao, *J. Phys. Chem. C* **2009**, *113*, 1001–1005.
- [20] S. A. C. Carabineiro, *Front. Chem.* **2019**, *7*, 702.
- [21] N. G. Bastús, J. Comenge, V. Puentes, *Langmuir* **2011**, *27*, 11098–11105.
- [22] K. Zhang, W. Wang, W. Cheng, X. Xing, G. Mo, Q. Cai, Z. Chen, Z. Wu, *J. Phys. Chem. C* **2009**, *114*, 41–49.
- [23] K. Shen, C. Jia, B. Cao, H. Xu, J. Wang, L. Zhang, K. Kim, W. Wang, *Electrochim. Acta* **2017**, *256*, 129–138.
- [24] R. Banerjee, D. Ghosh, J. Satra, A. B. Ghosh, D. Singha, M. Nandi, P. Biswas, *ACS Omega* **2019**, *4*, 16360–16371.
- [25] S. Möller, S. Barwe, J. Masa, D. Wintrich, S. Seisel, H. Baltruschat, W. Schuhmann, *Angew. Chem. Int. Ed. Engl.* **2020**, *59*, 1585–1589.
- [26] J. Hernández, J. Solla-Gullón, E. Herrero, A. Aldaz, J. M. Feliu, *Electrochim. Acta* **2006**, *52*, 1662–1669.
- [27] M. Avramov-Ivic, R. R. Adzic, A. Bewick, M. Razaq, *J. Electroanal. Chem. Interfacial Electrochem.* **1988**, *240*, 161–169.
- [28] M. Haruta, A. Ueda, S. Tsubota, R. M. Torres Sanchez, *Catal. Today* **1996**, *29*, 443–447.
- [29] N. Mayet, K. Servat, K. B. Kokoh, T. W. Napporn, *Electrocatalysis* **2021**, *12*, 26–35.
- [30] J. Zhang, P. Liu, H. Ma, Y. Ding, *J. Phys. Chem. C* **2007**, *111*, 10382–10388.
- [31] A. B. Anderson, H. A. Asiri, *Phys. Chem. Chem. Phys.* **2014**, *16*, 10587–10599.
- [32] S. S. Sarmoor, S. J. Hoseini, R. Hashemi Fath, M. Roushani, M. Bahrami, *Appl. Organomet. Chem.* **2018**, *32*, e3979.
- [33] S. Yan, S. Zhang, *Int. J. Hydrogen Energy* **2011**, *36*, 13392–13397.
- [34] Y. Liu, H. Yang, X. Li, L. Mao, *Mater. Lett.* **2013**, *106*, 287–289.
- [35] J. Xian, Q. Hua, Z. Jiang, Y. Ma, W. Huang, *Langmuir* **2012**, *28*, 6736–6741.
- [36] J. Luo, M. M. Maye, N. N. Kariuki, L. Wang, P. Njoki, Y. Lin, M. Schadt, H. R. Naslund, C.-J. Zhong, *Catal. Today* **2005**, *99*, 291–297.
- [37] K. Sun, T. Cheng, L. Wu, Y. Hu, J. Zhou, A. MacLennan, Z. Jiang, Y. Gao, W. A. Goddard, Z. Wang, *J. Am. Chem. Soc.* **2017**, *139*, 15608–15611.
- [38] C. Rogers, W. S. Perkins, G. Veber, T. E. Williams, R. R. Cloke, F. R. Fischer, *J. Am. Chem. Soc.* **2017**, *139*, 4052–4061.

Manuscript received: March 2, 2022  
 Revised manuscript received: April 7, 2022  
 Accepted manuscript online: April 8, 2022  
 Version of record online: May 5, 2022